JOURNAL OF APPLIED CRYSTALLOGRAPHY

Volume 50 (2017)

Supporting information for article:

EBSD STUDY OF ORIENTATION GRADIENTS AT THE GRAIN BOUNDARIES OF A POLYCRYSTALLINE STEEL SHEET DEFORMED ALONG DIFFERENT LOADING PATHS

J. W. Signorelli, A. Roatta, N. De Vincentis, C. Schwindt, M. Avalos, R. E. Bolmaro and N. Bozzolo

Supplementary Material for:

EBSD study of orientation gradients at the grain boundaries of a polycrystalline steel sheet deformed along different loading paths

J.W. Signorelli, A. Roatta, N. De Vincentis, C. Schwindt, M. Avalos, R.E. Bolmaro, N. Bozzolo

Supplementary information about experimental procedure

Average Confidence Index and Average Image Quality for each EBSD maps are provided in Table S1. Both parameters show a very acceptable value, not being necessary to perform any cleanup procedure. However, in order to put in evidence how the cleanup procedure affects the evaluated EBSD-parameters a standard Grain Dilation with 5 degree of angular tolerance and a minimum grain size of 5 pixels and only 1 iteration was performed over the original EBSD maps. The observed variations between original and cleaned-up data were, in all cases, minimal and without relevant consequences on the subsequent values of the investigated magnitudes. A second Table S2 shows the details of the variations of the average of local gradient of crystal orientation ($G_{L\ ave}$); the background noise ($B_{L\ ave}$) and the kernel average misorientation (KAM_{ave}) for the original and cleaned-up EBSD maps. Also, for each scan the EBSD points that were changed by the procedure are detailed.

Table S1

	Size [μm]	# of points	Average Confidence Index	Average Image Quality
AR				
scan#1	39.90 x 83.74	386716	0.74	5837.42
scan#2	64.90 x 25.03	188355	0.71	5766.64
scan#3	99.90 x 49.71	574713	0.78	5619.11
scan#4	100 x 99.94	1155578	0.72	5319.06
scan#5	99.50 x 79.76	917851	0.73	5732.20
scan#6	100 x 99.94	1155578	0.79	5736.82
UAT				
scan#7	100 x 79.93	924462	0.79	3879.06
scan#8	110 x 69.97	890305	0.79	3973.13
scan#9	62 x 75	537974	0.79	4056.03
scan#10	55 x 49.97	318189	0.71	3741.31
scan#11	120 x 109.90	1524635	0.55	1290.54
scan#12	100 x 99.94	1155578	0.69	5709.31
PS				
scan#13	65 x 59.93	450797	0.64	3205.62
scan#14	65 x 59.93	450797	0.66	3203.38
scan#15	65 x 59.93	450797	0.65	3275.46
scan#16	100 x 99.94	1155578	0.81	5367.58
scan#17	100 x 99.94	1155578	0.80	5449.65
EBA				
scan#18	110 x 75	954134	0.69	1664.81
scan#19	65 x 64.95	488526	0.75	6146.87
scan#20	65 x 64.95	488526	0.71	5718.44
scan#21	99.60 x 45.03	519177	0.71	5268.54
scan#22	99.70 x 44.69	515708	0.67	5050.07

Table S2

				Cleaned-up			*Observation*
	GL_{ave}	**BL_{ave}**	**KAM_{ave}**	**GL_{ave}**	**BL_{ave}**	**KAM_{ave}**	*Changed EBSD points*
AR							
scan#1	0.249	0.297	0.338	0.253	0.296	0.338	2832
scan#2	0.241	0.299	0.337	0.245	0.298	0.36	1604
scan#3	0.339	0.306	0.368	0.344	0.306	0.366	8376
scan#4	0.328	0.32	0.389	0.331	0.32	0.390	21850
scan#5	0.362	0.292	0.364	0.365	0.295	0.364	6705
scan#6	0.224	0.316	0.351	0.226	0.322	0.35	6590
UAT							
scan#7	1.528	0.305	0.608	1.526	0.304	0.582	6236
scan#8	1.480	0.3	0.612	1.477	0.299	0.581	7581
scan#9	1.021	0.289	0.51	1.018	0.288	0.488	3386
scan#10	1.263	0.344	0.615	1.257	0.342	0.617	5305
scan#11	1.301	0.353	0.627	1.307	0.355	0.627	16879
scan#12	1.482	0.255	0.542	1.486	0.257	0.546	10163
PS							
scan#13	1.296	0.319	0.605	1.294	0.318	0.574	3431
scan#14	1.093	0.309	0.537	1.09	0.308	0.517	2429
scan#15	1.331	0.309	0.564	1.329	0.307	0.566	3432
scan#16	1.106	0.26	0.467	1.106	0.261	0.468	7047
scan#17	1.122	0.265	0.473	1.121	0.26	0.474	6141
EBA							
scan#18	2.075	0.352	0.781	2.072	0.346	0.691	22091
scan#19	2.235	0.358	0.789	2.233	0.355	0.751	5223
scan#20	2.308	0.372	0.771	2.307	0.366	0.772	7363
scan#21	2.518	0.365	0.823	2.52	0.371	0.824	6845
scan#22	2.361	0.327	0.758	2.361	0.327	0.758	11160

In order to give more information about material microstructure, the next supplementary figure (Fig. S1) shows the Image Quality maps obtained for the analyzed samples. Boundaries are highlighted according to their misorientation.

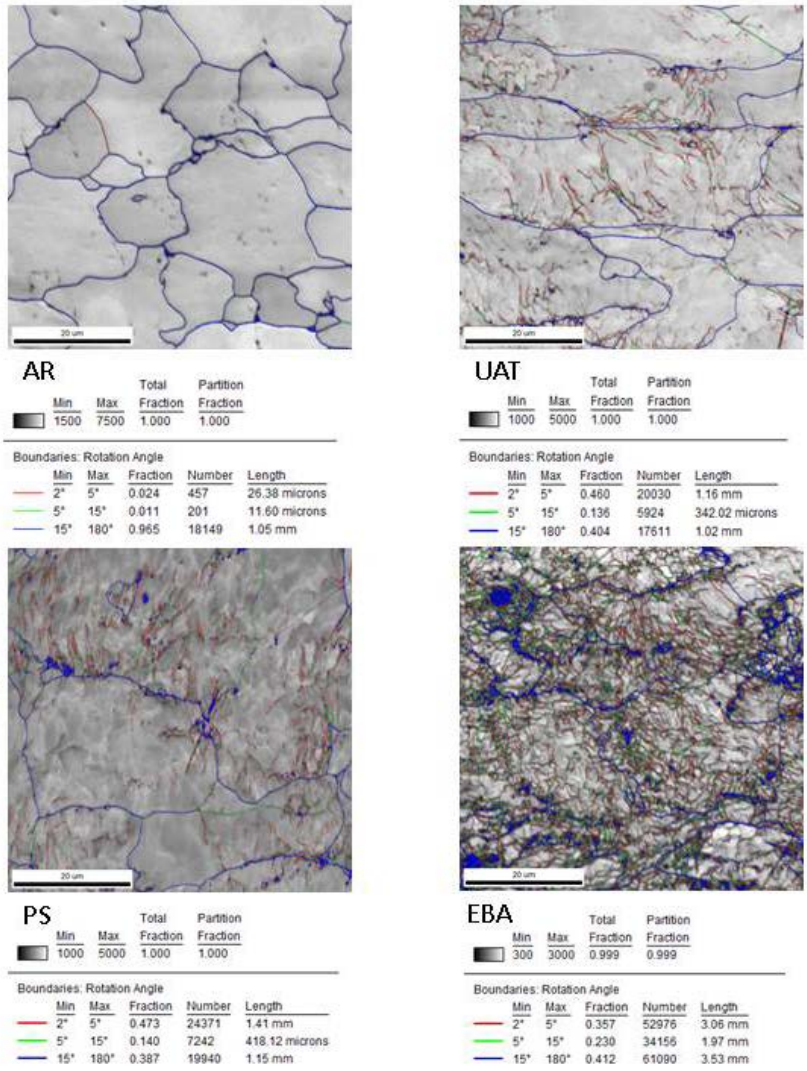

Figure S1. Image Quality maps with boundaries highlighted according to their misorientation

Supplementary information about definitions of points for calculation of extended local misorientation

The extended local misorientation for a given pixel i, as it is described by equation (2) follows Kamaya's, 2011 convention. Figure S2 shows the five first neighbor layers within a hexagonal grid.

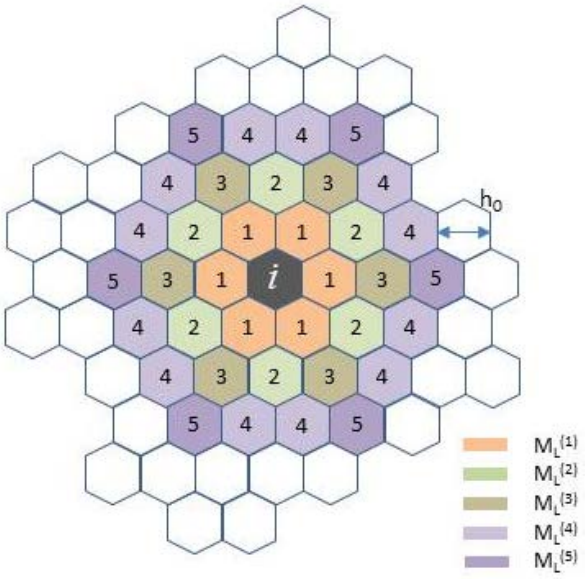

Figure S2. Neighborhoods considered for defining the extended local misorientation within a hexagonal grid.

Supplementary information about the influence of higher number of kernel sizes

To assess the influence of number of kernel sizes we extended the analysis up to 8th neighbors (i.e. pass from a range of up to 3 µm to a range of approximately 4.5 µm.). The following two plots resume the effect over the local gradient misorientation G_L. The example corresponds to the EBSD maps (#13) obtained after plain-strain stretching. The two graphs are complementary: the left one compares the histogram evaluated from G_L data obtained by least squares fitting over 5 M_L factors with the corresponding ones over 8 M_L factors. The extended local misorientation up to a number of kernel sizes of 8^{th} neighbors produces a shift (increase) of the G_L distribution for low and intermediate values, being indistinct for large G_L values. The right plot shows a one-to-one comparison of the G_L evaluated using a number of kernel sizes of 5 or 8 respectively. While it is not the ideal situation, a particular pattern is not observed but rather a dispersion of values around the line of equality (G_L(# 5) = G_L(# 8)).

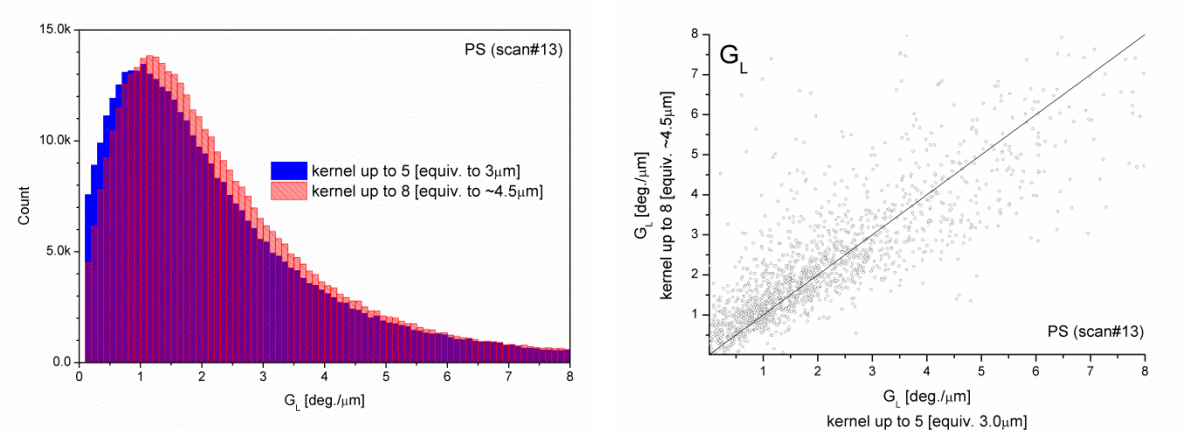

Figure S3. Influence of number of kernel sizes. Distribution of the local gradients of crystal orientations

Supplementary information about the proposed model profile

The proposed model requires the application of a linear regression procedure on the misorientation data in the vicinity of each GB in order to consider that a misorientation profile can be described accurately by a line with negative slope from the GB to the grain interior. Results were calculated assuming a threshold of $R^2 > 0.75$. Since this value was chosen almost arbitrarily, it is appropriate to analyze the effects of changing this threshold to less, $R^2 > 0.60$, and more restrictive conditions, $R^2 > 0.90$, respectively (Fig. S4). As expected, as the requirement to be satisfied is higher, the GBZ number that verifies the criterion decreases. Moving from a value of 794 (over a total of 1677) to 890 for a weak correlation coefficient of 0.60 and diminished to 565 if the $R^2 = 0.90$.

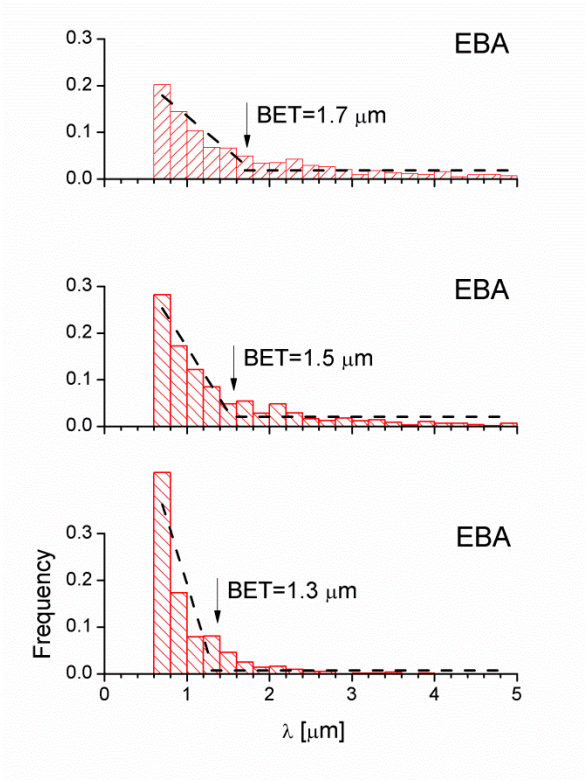

R^2 = 0.60
(number of identified GBZ: 890)

R^2 = 0.75
(number of identified GBZ: 794)

R^2 = 0.90
(number of identified GBZ: 565)

Figure S4. Distribution of effective thickness λ for the admissible GB profiles after EBA stretching.

Additionally, the analysis of two populations described in Figure 8 has been extended to all tested conditions and it is possible to see that these differences (even for the AR sample) are similar.

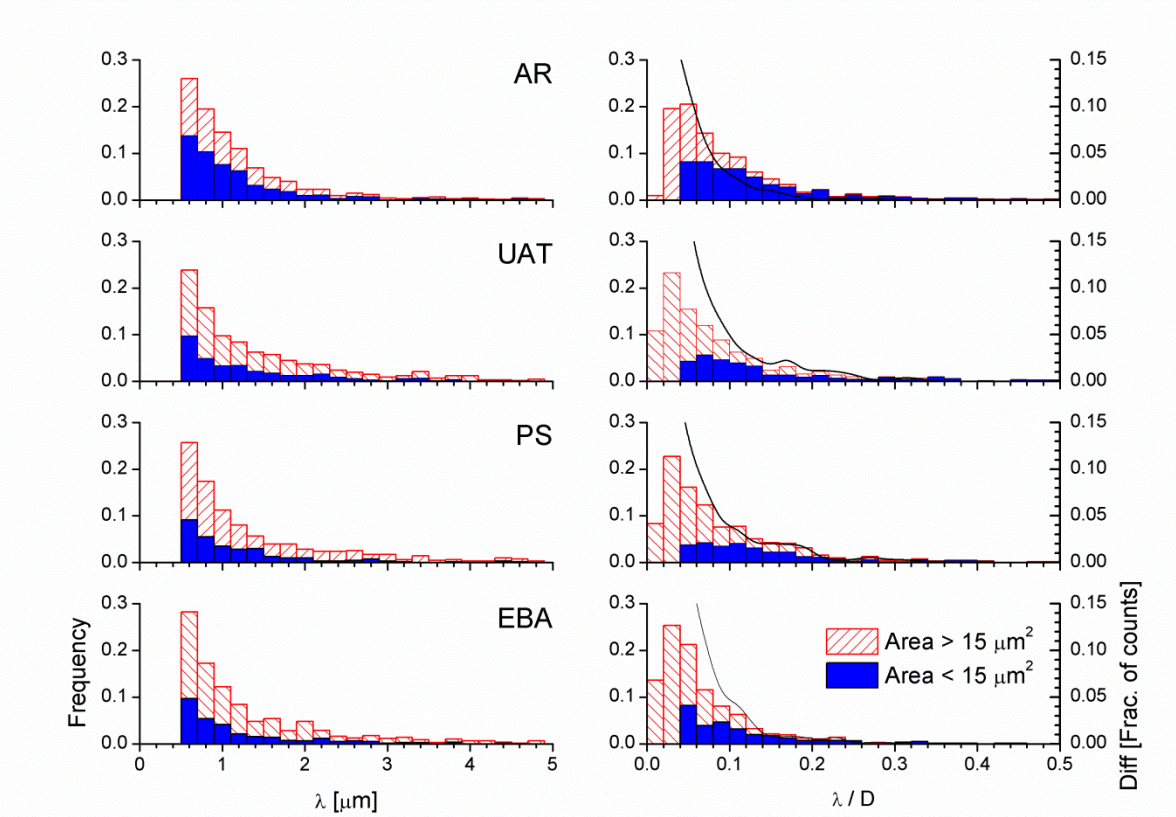

Figure S5: Distribution of effective thickness λ (left) and λ/D (right) for all admissible GB profiles based on the average of local misorientations. Stripped and solid bars identify the fraction of GB profiles with a given value of λ/D with apparent diameter greater and lesser than 15 μm, respectively. Solid lines in the right graphs indicate the difference between both populations in terms of fraction of counts per bin.